Interaction effects on microwave-assisted switching of $Ni_{80}Fe_{20}$ nanowires in densely packed arrays

Jesco Topp and Detlef Heitmann
Institut für Angewandte Physik und Mikrostrukturforschungszentrum, Universität Hamburg, Jungiusstrasse 11, D-20355 Hamburg, Germany

Dirk Grundler*
Physik Department, Lehrstuhl für Physik funktionaler Schichtsysteme, Technische Universität München, James-Franck-Str. 1, D-85747 Garching b. München, Germany
(Received 9 June 2009; published 24 November 2009)

We perform broadband microwave absorption spectroscopy and explore the switching behavior of 300-nm-wide and 20-nm-thick $Ni_{80}Fe_{20}$ nanowires under irradiation of a magnetic rf field. In particular, we investigate two arrays where the nanowires exhibit a different edge-to-edge separation, $a=100$ and 700 nm. In the arrays we observe microwave-assisted switching (MAS). The MAS process with a resonant behavior near 6 GHz is attributed to the excitation of a confined Damon-Eshbach-type mode. Dipolar interactions between nanowires are found to decrease the optimum frequency for MAS and to increase the switching efficiency for the small separation a. The observed characteristics are substantiated by model considerations. We propose a modification of the previously introduced analytical demagnetization factors of an individual thin wire and incorporate the effect of dipolar interactions occurring in the array. The approach explains the dependence of the MAS-relevant eigenmode on the edge-to-edge separation a. MAS is also found to narrow the switching field distribution of the nanowire array.

DOI: 10.1103/PhysRevB.80.174421 PACS number(s): 75.75.+a, 76.50.+g, 75.30.Ds, 75.50.Bb

I. INTRODUCTION

Magnetization reversal in micron and submicron sized ferromagnetic structures is a field of on-going research. A fundamental understanding of reversal processes on the subnanosecond time scale and in the GHz frequency regime is required to optimize switching and data transfer rates in magnetic storage devices. As the lateral size of ferromagnetic nanostructures decreases, quasistatic switching fields $H_{s,static}$ in general increase. To induce the switching at still moderate Oersted fields different techniques are currently explored. Among them there is heat-assisted magnetization reversal. Here, one obtains small switching fields H_s by locally increasing the temperature, e.g., via heating by a focused laser. A further approach is called microwave-assisted switching (MAS) (also named microwave-assisted magnetization reversal). In this technique, radio-frequency magnetic fields are irradiated on the ferromagnet to overcome the energy barrier between two stable magnetic states via large-angle spin precession. It has recently been demonstrated that continuous-wave irradiation reduces the absolute value of the switching field of an individual magnet to a value below $|H_{s,static}|$.[1–4] The microscopic nature of the nonlinear spin excitations responsible for the switching is a topic of current interest.[5,6] MAS for densely packed arrays of nanomagnets is largely unexplored and the role of dipolar coupling between neighboring nanomagnets for such switching processes is unclear. Conceptionally one should distinguish between the impact of static and dynamic dipolar couplings. Detailed information on these issues is needed if MAS should play a role in magnetic recording where high-density integration of magnetic bits is relevant.

In this paper, we report experimental studies on MAS in 180-μm-long, 300-nm-wide $Ni_{80}Fe_{20}$ (Permalloy) nanowires. For nanowires with such a large aspect ratio, the longitudinal direction corresponds to the easy axis.[7] The spin-wave spectra of longitudinally magnetized wires have already been studied and confined Damon-Eshbach (DE) modes have been observed.[8] The magnetization **M** can be assumed to be either parallel or antiparallel to a field **H** applied along the easy axis. We will denote the two configurations of **M** in the following as *down* (parallel) and *up* (antiparallel) configurations. In the following we will discuss the reversal in negative fields H which we assume to point *downward* in Figs. 1(b) and 1(c). The experiments are performed on arrays of nominally identical nanowires. Nevertheless we observe a significant distribution of quasistatic switching fields which we attribute to unintentional edge roughness. We find that the switching to the parallel (down) state is induced by microwave irradiation at characteristic frequencies even if the absolute value of H is still smaller than $|H_{s,static}|$ which is the quasistatic reversal field averaged over the array. The eigenmode that prominently triggers the magnetization reversal is found to be the confined DE mode of lowest order when driven into the nonlinear regime. Overall we encounter a reduction of switching fields of 60% by microwave irradiation. In the arrays we find that dipolar interactions between nanowires significantly reduce the critical microwave field h_{crit} that is necessary to trigger the reversal. We remodel this behavior using a macrospin approximation, which allows us to consider the influence of the dipolar stray field between nanowires. We adapt the previously introduced analytical demagnetization factors of an individual thin wire[9] and incorporate the effects of dipolar interactions. This approach allows us to explain the observed dependence of MAS on the separation a. At the same time the distribution of switching fields is found to narrow. The observations are

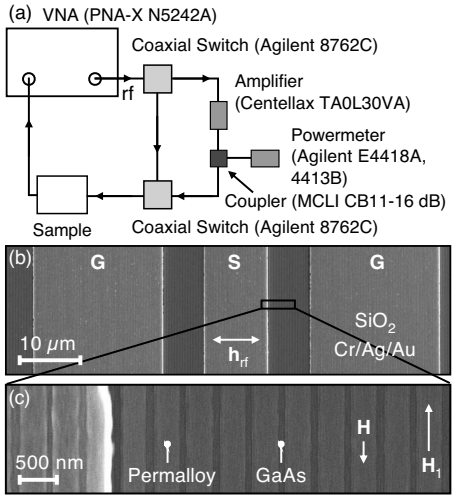

FIG. 1. (a) Sketch of the experimental setup. Two computer controlled coaxial switches allow us to use two different signal paths for the microwaves without disconnecting coaxial cables. The signal path which is not in operation is terminated with 50 Ω. In one path the microwaves are guided directly to the sample. In the other path they are first amplified by approximately 30 dB and second guided to the sample. Using a 16 dB directional coupler we measure the power of the microwaves at each frequency before the signal path to the sample is in operation. (b) Scanning electron microscopy image of sample A showing the CPW consisting of ground-signal-ground (G-S-G) leads. (c) Zoom-in showing Permalloy wires ($w=300$ nm) with an edge-to-edge separation of $a=100$ nm.

relevant if MAS should be used for encoding magnetic information.

The paper is organized as follows. In Sec. II we describe the investigated sample design and introduce the experimental technique of microwave absorption spectroscopy which we used to study the switching behavior. The experimental results are presented in Sec. III and in Sec. IV we discuss our findings and develop a theoretical model to describe the discovered effects.

II. EXPERIMENTAL TECHNIQUES: NANOLITHOGRAPHY AND SPIN-WAVE SPECTROSCOPY

The nanowires were prepared from $d=20$-nm-thick thermally evaporated Permalloy. Ferromagnetic resonance measurements on the unpatterned film yielded a saturation magnetization $\mu_0 M_{\mathrm{sat}}=1.12$ T with negligible anisotropy. Following Ref. 10 the phenomenological damping constant α was determined from the power-absorption linewidth as $\alpha=0.006\pm0.001$. Electron-beam lithography at 30 kV was used in conjunction with a polymethyl methacrylate (PMMA) 50 K/950 K double-layer resist and a lift-off process to generate $w=(300\pm10)$-nm-wide and 180-μm-long wires with an edge-to-edge distance of either $a=100\pm10$ nm (sample A) or $a=700\pm10$ nm (sample B). Details of the fabrication process can be found in Ref. 11. The arrays in this paper had $N=450$ wires in total for sample A and $N=10$ for sample B. Coplanar waveguides (CPWs) were used to guide microwave magnetic fields to the sample. These were prepared on top of the nanowire arrays. We positioned the CPWs in parallel with the nanowires. Both the in-plane and out-of-plane components of the rf field h_{rf} were orthogonal with respect to M when it was collinear with the easy axis. By this means we optimized the torque $\mathbf{M}\times\mathbf{h}_{\mathrm{rf}}$ to induce spin precession through the microwave field.

SiO_2 of 50 nm thick was used as an insulating intermediate layer. We fabricated the CPW from a 150-nm-thick trilayer of Cr/Ag/Au. The central conductors (gaps) had a width $w_{\mathrm{CPW}}=10$ μm ($\Delta_{\mathrm{CPW}}=6$ μm). The CPW was optimized to an impedance of $Z_0=50$ Ω. Previous experiments on transversally magnetized wires of similar lateral width showed that such wires did not exhibit measurable dipolar interaction at 700 nm edge-to-edge separation.[11] In sample B the overall dipolar interaction is at minimum due to both the large wire-to-wire distance a and the intentionally small number of wires ($N=10$ if compared to $N=450$ for sample A). For the longitudinally magnetized wires as discussed here we assume in the following that sample A (B) reflects an array consisting of dynamically interacting (noninteracting) nanowires.

The detection of spin-wave excitations was accomplished by broadband microwave absorption measurements. We used a vector network analyzer (VNA) to measure the microwave transmission T through the CPW in dependence of a sweep of the microwave frequency f.[12] CPW and VNA were connected through coaxial cables and microwave probes. For spin-wave spectroscopy in the linear regime a microwave with a small amplitude of $\mu_0 h_{\mathrm{rf}}\leq0.1$ mT was chosen to avoid unintentional nonlinear effects.[3] Resonant magnetic excitations resulted in a decreased microwave transmission due to absorption of power from the CPW at the eigenfrequency f of an excited spin wave (SW). We recorded spectra $T(f)$ at different in-plane magnetic fields $\mathbf{H}$. From each spectrum we subtracted a reference spectrum recorded at $\mu_0|\mathbf{H}|=90$ mT applied along the nanowire's easy axis. At such a high field spin-wave resonances were at frequencies well above 10 GHz and therefore outside the region of interest. The resulting difference spectrum $\Delta T(f)$ reflected the dynamic magnetic susceptibility $\chi(f)$ of the nanowires and, in particular, resonances due to SW excitation. A special rf calibration procedure such as TRL or SOLT calibration was not necessary. Details on the difference technique can be found in Refs. 10 and 13. A typical spectrum is shown in Fig. 2(b).

It is instructive to consider the wavelength λ of the excited SWs. For sample B the nanowires of number $N=10$ are well separated and present only below the inner conductor of the CPW. Here the in-plane component of h_{rf} is almost uniform and independent of the spatial coordinate. The amplitude is given by $\mu_0 h_{\mathrm{rf}}=\mu_0\sqrt{P/(4Z_0w^2)}$, with P being the rf power in watts.[3,13] A pronounced out-of-plane component occurs only close to the CPW edges and in the gap where no nanowires exist. We expect SW excitations in sample B to be in the long-wavelength limit, i.e., the wave vector $q=2\pi/\lambda$ transferred by the CPW microwave field is nearly zero. For sample A the scenario is somewhat different. The array covers an area of 180×180 μm^2 and extends beyond the CPW in transverse direction. It has recently been shown that an array of densely packed nanowires can form a so-called one-

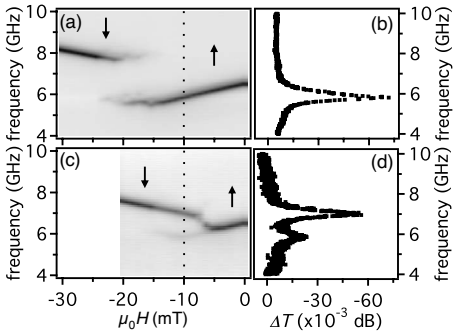

FIG. 2. (a) Spin-wave spectroscopy on sample A in the linear regime without prior rf irradiation. In the grayscale-coded microwave transmission spectrum light gray (black) denotes high (low) transmission. The abrupt change in the magnetic field dependence of the resonance frequency reflects irreversible switching of the wires. Arrows pointing up or down indicate the magnetization orientation. (b) Single spectrum taken from (a) at $\mu_0 H=-10$ mT [indicated by the *dotted* line in (a)]. (c) Microwave transmission spectrum *after* irradiation with a broadband microwave magnetic field where the frequency was varied between 2 and 10 GHz. The irreversible switching is found at a much smaller absolute value of H if compared to graph (a). As we focus on switching phenomena in this paper no further data were taken at $\mu_0 H<-22$ mT. (d) Single spectrum taken from (c) at $\mu_0 H=-10$ mT [indicated by the dotted line in (c)]. We note that the noise level in (c) is larger than in (b) because here we used the active signal path for spin-wave spectroscopy in the linear regime. For further experiments we switched to the passive path for taking spectra.

dimensional (1D) magnonic crystal exhibiting Brillouin zones and collective SW excitations with $q\neq 0$ in transverse direction.[14] In sample A, the number of nanowires is $N=450$, and they are densely packed. This leads to a considerable number of nanowires in the gaps and under the ground leads of the CPW. The array is thus subject to the nonuniform h_{rf}. This might allow us to excite collective SWs with a finite wave vector. To estimate the transferred wave vector in transverse direction one needs to perform a Fourier analysis of the spatial profile of h_{rf}. For our CPW we estimate the prominent component to exhibit a wave vector of $q=2\pi/(w_{\mathrm{CPW}}+2\Delta_{\mathrm{CPW}})\approx 2900$ rad/cm.[15] This value is far smaller than the boundary of the first Brillouin zone, i.e., $\pi/(w+a)=79\,000$ rad/cm. The experiment on sample A is thus still in the long-wavelength limit. Additionally performed micromagnetic simulations substantiate our conclusion.

In this paper we present four different kinds of experiments on the nanowire arrays. For this we make use of two separate signal paths, i.e., a "passive" and an "active" path where only the latter one incorporates a microwave amplifier. A sketch of the wiring is displayed in Fig. 1(a). For each experiment the relevant path is predefined using remotely controlled coaxial switches. First we will show data obtained by spin-wave spectroscopy in the linear regime [cf. Fig. 2(a)]. Here the VNA power is always at a small level and the passive signal path without the amplifier is used. Second we will demonstrate the existence of MAS in sample A due to *broadband* microwave irradiation. For this we set the biasing field H, irradiate the sample using maximum VNA output power at frequencies ranging from 2 to 10 GHz, and then perform spin-wave spectroscopy in the linear regime [cf. Fig. 2(c)]. This experiment is performed using the active signal path. Third we will discuss irradiation experiments where we explore in detail the MAS process as a function of both irradiation frequency and rf field amplitude at a specific biasing field H. Here the active signal path incorporating the amplifier is used to irradiate the sample under well-defined conditions before we switch to the passive signal path and perform spin-wave spectroscopy in the linear regime to test the magnetic configuration of the nanowires after each irradiation step. From such data we calculate the MAS yield and determine the frequency dependence of the critical microwave field amplitude which initiates the switching. The active signal path is also used for the fourth set of experiments by which we explore the MAS yield as a function of biasing field H at a fixed irradiation frequency.

III. MICROWAVE-ASSISTED SWITCHING OF INTERACTING NANOWIRES (SAMPLE A)

In the following we present the experimental data obtained on sample A. We focus on the array of interacting nanowires (sample A) since MAS of noninteracting nanowires (sample B) has recently been reported in Ref. 16.

A. Demonstration of MAS in a broadband rf field

In Fig. 2 we compare field-dependent spin-wave spectroscopy on sample A (separation $a=100$ nm) without (a) and with (c) broadband microwave irradiation prior to the transmission measurement. Before we applied a negative H we aligned all wires in a positive field (configuration up). This is done for every measurement in order to have a well-defined starting point for the switching experiments. The nonirradiated wires in (a) exhibit the up state for $\mu_0 H>\mu_0 H_{\mathrm{s,i}}=-14$ mT. Figure 2(b) shows a single transmission spectrum taken at $\mu_0 H=-10$ mT with small VNA power $P=-10$ dBm, i.e., in the linear regime.[3] We observe a pronounced resonance at 5.8 GHz. Considering the long-wavelength limit of our excitation we attribute the resonance to a standing SW mode which is confined in transverse direction in each of the wires. It corresponds to the quantized Damon-Eshbach mode of the lowest order.[8] The mode features a wave crest in the center of the individual wire. It has been shown that the transverse wave vector should fulfill boundary conditions originating from dipolar pinning.[17] The dynamical pinning determines the so-called effective width w_{eff} of the magnetic wire where the nodes exist. w_{eff} determines the eigenfrequency. Below we will show that neighboring nanowires change the eigenfrequency of this mode in a densely packed array.

Decreasing H below $H_{\mathrm{s,i}}$ leads to a discontinuous jump in eigenfrequency and an abrupt change of the slope. These features indicate the irreversible switching of nanowires. Nanowires in the down state exhibit a larger eigenfrequency than in the up state.[12] Due to the distribution of reversal fields in the array the intensities of the corresponding absorption lines do not change abruptly by 100% at $H_{\mathrm{s,i}}$ but gradu-

ally vanish and appear with H between $\mu_0 H_{s,i}=-14$ mT and $\mu_0 H_{s,f}=-23$ mT. The averaged quasistatic reversal field thus amounts to $\mu_0 H_{s,static}=-18.5$ mT. In this work we use negative values for the switching fields to highlight that the reversal occurs in the opposing field if compared to the initial state. This is true for quasistatic reversal and MAS processes.

For Fig. 2(c) the nanowires had been irradiated with high-power microwaves before the transmission spectra were taken at $P=-10$ dBm. We did not use at a single frequency for the irradiation but swept f between 2 and 10 GHz in steps of $\Delta f=6.2$ MHz; the irradiation time was 1 μs per step with a power of $P\approx 23$ dBm. This was the maximum attainable power (corresponding to a field amplitude $\mu_0 h_{rf}\approx 3.5$ mT). The experiment was done by choosing the transmission line with the amplifier [cf. Fig. 1(a)]. After irradiation a low-power spin-wave spectrum was recorded. At -10 mT we now find two resonances in Fig. 2(d); a weak one at 5.8 GHz and a strong resonance at 7.0 GHz. This resonance at higher frequency originates from those wires that have reversed their magnetization and aligned with the applied field, i.e., they reversed from the up to the down state due to *microwave irradiation*. Most of the wires reversed such that the intensity at the higher frequency is markedly more pronounced if compared to the resonance at low frequency. The MAS process sets in at -7 mT. Thus the reversal field of nanowires has been changed by 50% if compared to $\mu_0 H_{s,i}=-14$ mT. The resonance frequency of the reversed wires increases with decreasing field, i.e., increasing $|H|$. The transition between the two branches of different slopes is sharper in Fig. 2(c) if compared to Fig. 2(a). For $\mu_0 H<-7$ mT we observe a faint residual resonance at low frequencies in Fig. 2(c). We attribute this weak absorption line to wires which reside far too left and right of the CPW. There the rf amplitude is too small to induce the magnetization reversal. For $\mu_0 H\leq -15$ mT this parasitic resonance feature is no longer resolved. Comparison between Figs. 2(a) and 2(c) shows that (i) the absolute field needed to switch the nanomagnet is reduced by about a factor of 2 and (ii) the switching field distribution is much narrower than without irradiation. This second aspect is relevant in magnetic recording where one aims at the same switching field for all the magnetic bits.

B. Frequency vs rf field dependency

In the following we explore in detail the microwave-assisted switching process and present experimental MAS regime diagrams. For this we determine the switching yield as a function of the well-defined frequency and amplitude of the rf irradiation. We used two rf coaxial switches and the active path in which the output signal of the VNA was amplified by 30 dB before being guided to the sample. The exact rf power was measured by a rf power meter connected to a 16 dB directional coupler. The rf power was adjusted with an accuracy of 0.05 dB before each individual irradiation. During the adjustment of the power level the rf line was terminated with 50 Ω such that the sample remained undisturbed. The termination was removed only after the correct power level was stable. We also considered the damping and characteristic frequency response of the directional coupler,

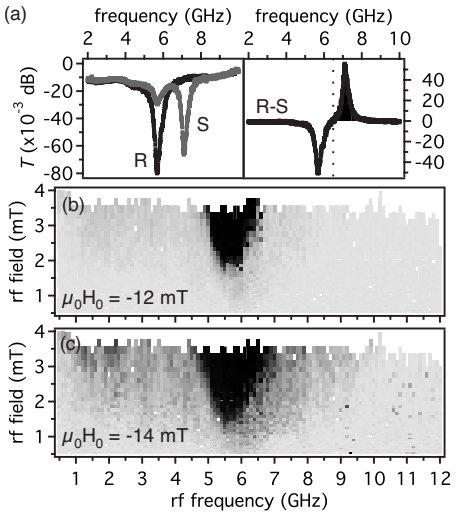

FIG. 3. (a) Left: spectra measured on sample A at $P=-10$ dBm and $\mu_0 H=-12$ mT after two different irradiation experiments: the curve $R(S)$ corresponds to irradiation at $f=0.5$ GHz and $P=5$ dBm ($f=5.3$ GHz and $P=19$ dBm). Only spectrum S reflects microwave-assisted switching. Right: difference signal $R-S$; the area under the curve colored in black is proportional to the number of nanowires that reversed due to MAS. This area is a measure of the switching yield. (b) Switching-yield diagram MAS(f,h_{rf}) for the microwave-assisted switching at $\mu_0 H_0=-12$ mT [light gray (black) denotes 0% (100%) yield]. White indicates regions where no data points were recorded due to the frequency-dependent maximum output power of the rf amplifier. (c) Switching-yield diagram MAS(f,h_{rf}) at $\mu_0 H_0=-14$ mT (which is at the onset of quasistatic switching at $H_{s,i}$).

the cables, and the rf microwaves. We thoroughly investigated their performance using the VNA. The values given in this paper represent the upper boundary for the power sent to the magnets because we did not correct for the residual damping of the impedance-matched CPW. Before each measurement the nanowires were magnetized along the easy axis with $\mu_0|\mathbf{H}_1|=50$ mT to generate uniform up orientation. The microwave power was "on" for a duration of 1.3 s (Ref. 18) at an applied field $H<0$ which was larger than the averaged negative quasistatic switching field $\mu_0 H_{s,static}=-18.5$ mT, i.e., the nanowires' magnetization $\mathbf{M}$ was mostly up prior to irradiation. After irradiation, we measured a spin-wave spectrum at small VNA power $P=-10$ dBm, i.e., in the linear regime. This experiment was repeated for different combinations of f and amplitudes h_{rf}. The spectrum of nanowires in the initial configuration served as a reference spectrum. Such a spectrum is labeled by R in Fig. 3(a). Here a pronounced resonance at a low frequency of 5.7 GHz is found at $\mu_0 H_0=-12$ mT. Depending on f and h_{rf} characteristic changes in the spin-wave spectrum occurred. A typical spectrum labeled by S is depicted in Fig. 3(a). In addition to the resonance at 5.7 GHz we observe a further one at 7.1 GHz indicating that nanowires had switched due to MAS. We used the signal strength of this resonance to quantify the number of nanowires in the down state. For this we evaluated the difference spectra $R-S$ as shown in Fig. 3(a) on the right-hand side.[19] The relative number of switched nanowires was calculated from the integral of the high frequency peak (filled with

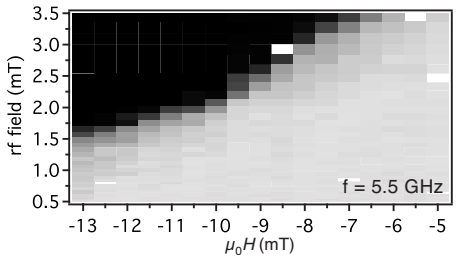

FIG. 4. Switching-yield diagram MAS(H,h_{rf}) of sample A for microwave irradiation at a fixed frequency of f=5.5 GHz [light gray (black) denotes 0% (100%) yield and white indicates no data points].

black color). The maximum switching yield was defined as 100% for a spectrum measured at very large amplitudes h_{rf}, although some residual intensity remained with the low-frequency mode. This residual intensity was independent of the exact irradiation power. We attributed this signal to the nanowires which were too far away from both sides of the waveguide such that the local h_{rf} was below the threshold value for MAS and thus not sufficient to stimulate the reversal.

Figure 3(b) displays the switching-yield diagram MAS(f,h_{rf}) for $\mu_0 H_0$=−12 mT as a density plot; light gray (black) encodes low (high) yield. Data points which are missing due to the nonlinearity of the power amplifier are indicated in white. We find that for microwave fields up to $\mu_0 h_{rf} \approx 4$ mT the up state is stable against microwave irradiation in a broad frequency regime. Pronounced switching is observed for irradiation frequencies between 5 and 6.5 GHz. Here we find a clear boundary between the regimes of zero and maximum switching yield which suggests resonant behavior. At 5.5 GHz a critical microwave field of $\mu_0 h_{crit}$ =1.85 mT is sufficient to switch 90% of the nanowires to the down state. We studied MAS also at $\mu_0 H_0$=−14 mT. The corresponding switching-yield diagram is displayed in Fig. 3(c). Here the MAS efficiency at 5.5 GHz is larger, i.e., the $\mu_0 h_{crit}$ is reduced to below 1.85 mT. At the same time the frequency regime where MAS occurs has increased. A 90% switching yield is achieved in Fig. 3(c) by using $\mu_0 h_{crit}$ =1.5 mT at 5.4 GHz. The boundary between 5 and 6.5 GHz has become less well defined if compared to Fig. 3(b). We attribute this observation to the quasistatic reversal of individual nanowires since −14 mT=$\mu_0 H_{s,i}$. A detailed analysis of the data reveals two further MAS resonances near low frequencies of 1.3 and 2.2 GHz. The switching yield is up to 75% at $\mu_0 h_{rf}$=3.5 mT. These resonances will not be discussed in this paper.

C. Static and rf field dependency

To further quantify the reduction of the switching field H_s by microwave irradiation, we altered the experiment and investigated the MAS yield as a function of applied static field $\mu_0 H_0$ and rf field $\mu_0 h_{rf}$ at a fixed frequency of f=5.5 GHz. The resulting MAS(H,h_{rf}) switching-yield diagram is displayed in Fig. 4. The largest applied field for which we observe a significant MAS yield with f=5.5 GHz is $\mu_0 H_0$=

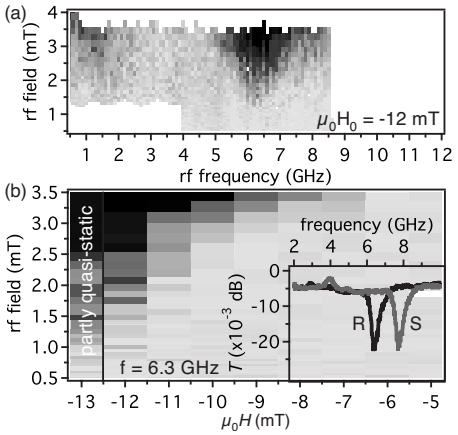

FIG. 5. (a) Switching-yield diagram MAS(f,h_{rf}) at $\mu_0 H_0$= −12 mT obtained on sample B where wires have a large edge-to-edge separation [light gray (black) denotes 0% (100%) yield and white indicates no data points]. Due to reduced number of nanowires in sample B the signal-to-noise ratio is lower. Each data point is the average of three successive irradiation experiments. (b) Switching-yield diagram MAS(H,h_{rf}) at a fixed frequency f =6.3 GHz. f was chosen such that $\mu_0 h_{rf}$ is minimal at $\mu_0 H$= −12 mT to induce the MAS process. Here, no averaging was used. For $\mu_0 H$<−12.5 mT wires begin to switch due to quasistatic reversal.

−6 mT. At $\mu_0 H_0$=−7.5 mT (−13 mT) the yield surpasses 90% for $\mu_0 h_{rf}$=3.5 mT (1.7 mT).

IV. MICROWAVE-ASSISTED SWITCHING OF NONINTERACTING WIRES (SAMPLE B)

So far we have discussed the results obtained on sample A where nanowires were separated by a=100 nm. To revisit the MAS for individual nanowires we investigated sample B where the edge-to-edge separation between nanowires of the same nominal width was a=700 nm. Quasistatic magnetization reversal occurred between $\mu_0 H_{s,i}$=−12.5 mT and $\mu_0 H_{s,f}$=−17.5 mT in this sample; the average switching field was $\mu_0 H_s$=−15 mT which is smaller than for sample A. This regime is also narrower if compared to sample A. Due to the reduced number of nanowires which are all located underneath the signal line of the CPW 100% switching yield can be achieved [see inset of Fig. 5(b)].

To switch nanowires of sample B from up to down by the MAS process at $\mu_0 H_0$=−12 mT amplitudes h_{rf} are found which are larger if compared to sample A. In Fig. 5(a) we need a critical microwave field of $\mu_0 h_{crit}$=2.7 mT at 6.3 GHz to switch 90% of the nanowires. This amplitude h_{crit} is a factor of 1.5 larger than for sample A. At the same time the optimum frequency for MAS is larger by $\Delta f \approx 800$ MHz [compare Fig. 3(c) and the inset of Fig. 5(b)]. The boundary is less well defined possibly due to the reduced number of nanowires. In Fig. 5(b) where we show a MAS(H,h_{rf}) switching-yield diagram for the fixed frequency of f =6.3 GHz the MAS yield surpasses 90% only for $\mu_0 H \leq$ −10 mT if compared to −7.5 mT in case of sample A.

At $\mu_0 H_0$=−12 mT we observe a resonant switching behavior also at low frequencies: at 1.2 GHz we obtain a high

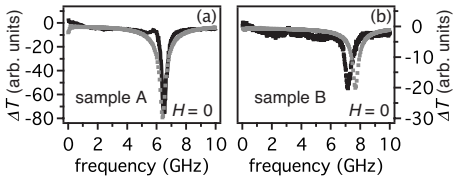

FIG. 6. (a) The black symbols depict the experimental spectrum taken on sample A at $H=0$. Gray symbols denote the spectrum obtained from micromagnetic simulations performed on an array consisting of 18 parallel nanowires of width $w=300$ nm, thickness $d=20$ nm, and with an edge-to-edge separation of 100 nm. (b) Experimental spectrum for $H=0$ obtained on sample B (black symbols) with large edge-to-edge separation. The resonance resides at higher frequency if compared to (a). Gray symbols denote the spectrum obtained from micromagnetic simulations performed on an individual nanowire of width $w=300$ nm and thickness $d=20$ nm.

switching yield of up to 75% in Fig. 5(a). The MAS process driven by this mode does not seem to depend on the edge-to-edge separation a between nanowires. Interestingly, we do not resolve this mode in the low-power spin-wave spectra. The microscopic nature of this mode should be explored in future studies. It is beyond the scope of this paper.

V. MODELING AND DISCUSSION

Comparing the experimental data obtained on samples A and B we have found that the MAS characteristics differ quantitatively: both the frequency of the DE type resonance and critical microwave field are significantly smaller for sample A than for sample B. In the following we will attribute the observed differences to dipolar interactions between nanowires. To substantiate this we will first report micromagnetic simulations (Fig. 6) and second discuss an analytical model (Fig. 7).

A. Micromagnetic simulations

Following Ref. 11 we have performed micromagnetic simulations. To model the spectrum of an individual nanowire at $H=0$ [Fig. 6(b)] we take the parameters $w=300$ nm and $d=20$ nm. We use the OOMMF micromagnetic code[20] and apply the 1D periodic-boundary-condition extension[21] to model an infinitely long magnetic wire. The simulated segment has $\Delta x \times \Delta y \times \Delta z$ equal to $300 \times 100 \times 19.5$ nm^3. The OOMMF discretization uses a cell of $5 \times 25 \times 6.5$ nm^3.[22] Starting from a quasistatic configuration where $\mathbf{M}$ is aligned with the easy axis we perform dynamic simulations to numerically calculate the eigenmode spectrum. For this a field pulse $\vec{h}_{\mathrm{rf}}$ with amplitude of 1 mT and temporal full width at half maximum value of 2.5 ps is applied. We tilt $\vec{h}_{\mathrm{rf}}$ by 45° off from the in-plane direction.[11] The simulated spectrum for sample B is displayed in Fig. 6(b). The discrepancy between the measured and simulated eigenfrequencies is attributed to unintentional edge roughness which occurs in the real wires and modifies the dynamic stray field. We have analyzed the spatially resolved discrete Fourier transform of $M_z(x,y)$ to gain the mode profile in transverse direction to the wire axis (not shown). The profile substantiates that the resonance originates from the confined Damon-Eshbach mode of lowest order.

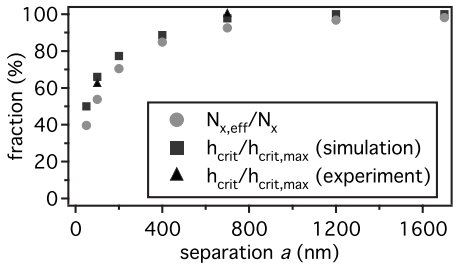

FIG. 7. Calculated effective demagnetization factors N_{eff}/N_x (full circles) and calculated critical microwave field $h_{\mathrm{crit}}/h_{\mathrm{crit,max}}$ for the onset of microwave-assisted switching (squares). The experimental results for $a=100$ nm and $a=700$ nm are displayed as triangles (these values are normalized to $h_{\mathrm{crit,max}}$ at $a=700$ nm).

To model the excitation of interacting nanowires we assumed an array of 18 parallel nanowires with an edge-to-edge separation of 100 nm. We find a very good agreement between the predicted spectrum and the experimental data obtained on sample A [Fig. 6(a)]. Comparing (a) and (b) we find that neighboring nanowires reduce the eigenfrequency of the SW mode. In the following we will develop an analytical model and discuss the microscopic mechanism.

B. Analytical model

To analytically model dipolar interactions in an infinite array of infinitely long wires we start in our calculations for sample A from a scenario where we assume a macrospin inside each wire. Thereby we model uniform precession dynamics which is roughly true for the confined DE mode of lowest order. We deliberately refrain from using a theoretical model based on a Green's function approach (see, e.g., Refs. 23 and 24) although it might provide more accurate eigenfrequencies and precession profiles. The macrospin approach, however, allows us both to highlight the underlying physics and to calculate the MAS boundary. In particular, it allows us to calculate a dipole-interaction induced correction to the well-known demagnetization coefficients for thin wires.[9]

The precessional motion of each macrospin is governed by the Landau-Lifshitz-Gilbert (LLG) equation,[25]

$$\frac{d\mathbf{m}}{dt} = -\gamma\mu_0[\mathbf{m} \times \mathbf{H}_{\mathrm{int}}] - \frac{\alpha\gamma}{M_{\mathrm{sat}}}[\mathbf{m} \times (\mathbf{m} \times \mathbf{H}_{\mathrm{int}})], \quad (1)$$

where $\mathbf{m}$ is the macrospin of a single wire per unit volume (γ is gyromagnetic ratio). In the following we assume the x direction to be transverse to the wire and the y direction along the wire, i.e., along the easy axis. The z direction is perpendicular to the plane. In equilibrium $\mathbf{m}$ points only in the y direction. The interaction between separated nanowires inside the array is of dipolar nature; therefore the interaction only needs to be included in the internal field H_{int} experienced by the macrospin,

$$\mathbf{H}_{\mathrm{int}}(t) = \mathbf{H} + \mathbf{h}_{\mathrm{rf}}(t) \tag{2}$$

$$- N_x m_x(t)\hat{\mathbf{e}}_x - N_z m_z(t)\hat{\mathbf{e}}_z \tag{3}$$

$$+ \mathbf{H}_{\mathrm{dip}}(t), \tag{4}$$

where $\mathbf{H}$ is the applied field, $\mathbf{h}_{\mathrm{rf}}(t)$ is the time-varying rf field, $N_{x(z)}m_{x(z)}(t)\hat{\mathbf{e}}_{x(z)}$ is the dynamic demagnetization fields in x and z directions due to the precession,[26] and $\mathbf{H}_{\mathrm{dip}}(t)$ is the stray field from the surrounding wires. Demagnetization effects in y direction can be neglected due to the assumed infinite length of the wire; the two remaining demagnetization factors can be approximated by[9]

$$N_x = \frac{2d}{\pi w}, \quad N_z = 1 - N_x. \tag{5}$$

The stray field in the plane of a wire ($z=0$) can be calculated by

$$H_{\mathrm{str},x}(x) = \frac{3}{4\pi}[wdm_x]\int_{-\infty}^{\infty} \frac{x^2 - \frac{1}{3}(x^2+y^2)}{(x^2+y^2)^{5/2}}dy \tag{6}$$

$$= \frac{1}{2\pi} wdm_x \frac{1}{x^2}, \tag{7}$$

where m_x is the x component of the unit macrospin. Inside an array of macrospins, which all perform the same precessional motion, the stray field becomes an infinite sum,

$$H_{\mathrm{dip},x}(t) = \frac{1}{2\pi} wdm_x(t) 2\sum_{n=1}^{\infty} \frac{1}{n^2(w+a)^2} \tag{8}$$

$$= \frac{\pi}{6}\frac{wd}{(w+a)^2} m_x(t), \tag{9}$$

with $w+a$ which is the period of the array. Equation (9) is only valid for discrete macrospins, i.e., a patterned film. For our evaluation the stray field in y (z) direction is neglected because of the infinite length (small thickness) of the nanowire. The field $H_{\mathrm{dip},x}$ is thus assumed to reflect the dipolar interaction in an infinite array of parallel nanowires. Both the outer stray field and the internal demagnetization field are proportional to the magnetization component m_x. They are, however, 180° phase shifted. We can combine these counteracting magnetic field effects by defining the effective demagnetization factor

$$N_{x,\mathrm{eff}} = N_x - \frac{\pi}{6}\frac{wd}{(w+a)^2}. \tag{10}$$

The minus sign accounts for the phase shift between demagnetization field and $H_{\mathrm{dip},x}$. For large separations a the second term in Eq. (10) approaches zero and the effective demagnetization factor becomes equal to N_x of the isolated wire. When nanowires get closer and closer the demagnetization effect in an applied transverse field H_x becomes less efficient due to neighboring wires and $N_{x,\mathrm{eff}}$ falls below N_x (full circles in Fig. 7). For $a=100$ nm we calculate $N_{x,\mathrm{eff}}/N_x = 54\%$ from Eq. (10), i.e., the demagnetization for a wire inside an array is reduced by about a factor of 2 if compared to the isolated wire. For $a=700$ nm the discrepancy is much less pronounced with $N_{x,\mathrm{eff}}/N_x = 92\%$.

We have observed that the eigenfrequencies of the DE modes in samples A and B differ by $\Delta f = 800$ MHz. If we now consider the reduced effective demagnetization according to Eq. (10) the Kittel formula for uniform spin precession[26] in nanowires would suggest $\Delta f = 1100$ MHz for the two different arrays (we take $\mu_0 M_{\mathrm{sat}} = 1.08$ T, $\gamma = 176$ GHz/T, and later on $\alpha = 0.01$). This value of Δf is in reasonable agreement with the experiment as the approach does not take into account both the spin-wave confinement in transverse direction and the inhomogeneous spin-precession profile.[17,27] We can consider this by adjusting the interaction strength to 75%. The reduced effective demagnetization for $a=100$ nm thus leads to a decrease in eigenfrequency of the DE mode in the densely packed nanowire array. At the same time, the reduced demagnetization effect allows for an increased spin-precession amplitude since dipolar pinning of spins at the edges is diminished.[27] For the same microwave field amplitude h_{rf} one thus expects a larger spin-precession cone angle for sample A than for sample B. The larger cone angle might facilitate the microwave-assisted switching in the densely packed array.

Solving the LLG equation Scholz and Batra[28] calculated MAS switching-yield diagrams for an isolated single-domain particle, i.e., a macrospin without neighbors. Our modeling now allows us to quantify the variation of h_{crit} with separation a. Therefore we solve the LLG equation by using an internal field derived from the demagnetization factors of Eq. (10). By this means we include the effect of neighboring wires. In Fig. 7 we show the calculated critical microwave fields (squares) for MAS. The values are normalized by $h_{\mathrm{crit}}/h_{\mathrm{crit,max}}$, where $h_{\mathrm{crit,max}}$ corresponds to $a=1700$ nm. h_{crit} varies by more than a factor of 2 in Fig. 7. Our experimental results for samples A with $a=100$ nm and B with $a=700$ nm (triangles) follow the predicted dependence on a. Simulation and experiment agree well. Reducing a thus systematically reduces h_{crit} and facilitates the microwave-assisted switching in densely packed arrays if compared to isolated nanowires.

VI. CONCLUSIONS

In conclusion, we investigated the MAS process in 300-nm-wide Permalloy nanowires. We found two regimes where microwave irradiation induces a magnetization reversal at reduced quasistatic fields. The MAS process induced by a Damon-Eshbach mode residing at high frequencies around 6 GHz was found to depend on the separation a between nanowires. Here dipolar interactions shifted the optimum frequency of MAS. At the same time the critical microwave field was decreased for small separations. In our case we found a decrease of up to 40% at $a=100$ nm. Under microwave fields of up to 4 mT the absolute value of the quasistatic switching field was reduced by more than 60% from 18.5 to 7 mT. We derived a model in which the dipolar interaction between the nanowires was included in a modified effective demagnetization coefficient. We observed a further

eigenmode that triggered the MAS process. This was at low frequencies around 1.2 GHz and did not seem to vary from array to array.

ACKNOWLEDGMENTS

The authors thank Sebastian Hankemeier, Andreas Krohn, Stefan Mendach, and Sandra Motl-Ziegler for fruitful discussions and Jan Podbielski for experimental support. This work was supported by the Deutsche Forschungsgemeinschaft via Grant No. SFB 668 and the German Excellence Cluster *Nanosystems Initiative Munich* (*NIM*). D.G. thanks the Max Planck Institute for the Physics of Complex Systems in Dresden, Germany, for the kind hospitality and support via "Magnon09: From Fundamentals to Applications."

*grundler@ph.tum.de

[1] C. Thirion, W. Wernsdorfer, and D. Mailly, Nature Mater. **2**, 524 (2003).
[2] H. T. Nembach, P. M. Pimentel, S. J. Hermsdoerfer, B. Leven, B. Hillebrands, and S. O. Demokritov, Appl. Phys. Lett. **90**, 062503 (2007).
[3] J. Podbielski, D. Heitmann, and D. Grundler, Phys. Rev. Lett. **99**, 207202 (2007).
[4] G. Woltersdorf and C. H. Back, Phys. Rev. Lett. **99**, 227207 (2007).
[5] F. Montoncello, L. Giovannini, F. Nizzoli, H. Tanigawa, T. Ono, G. Gubbiotti, M. Madami, S. Tacchi, and G. Carlotti, Phys. Rev. B **78**, 104421 (2008).
[6] R. Hertel and J. Kirschner, Physica B **343**, 206 (2004).
[7] B. B. Maranville, R. D. McMichael, C. L. Dennis, C. A. Ross, and J. Y. Cheng, IEEE Trans. Magn. **42**, 2951 (2006).
[8] J. Jorzick, S. O. Demokritov, C. Mathieu, B. Hillebrands, B. Bartenlian, C. Chappert, F. Rousseaux, and A. N. Slavin, Phys. Rev. B **60**, 15194 (1999).
[9] R. I. Joseph and E. Schlomann, J. Appl. Phys. **36**, 1579 (1965).
[10] S. Kalarickal, P. Krivosik, M. Wu, and C. E. Patton, J. Appl. Phys. **99**, 093909 (2006).
[11] J. Topp, J. Podbielski, D. Heitmann, and D. Grundler, Phys. Rev. B **78**, 024431 (2008).
[12] J. Podbielski, F. Giesen, M. Berginski, N. Hoyer, and D. Grundler, Superlattices Microstruct. **37**, 341 (2005).
[13] F. Giesen, J. Podbielski, and D. Grundler, Phys. Rev. B **76**, 014431 (2007).
[14] G. Gubbiotti, S. Tacchi, G. Carlotti, N. Singh, S. Goolaup, A. O. Adeyeye, and M. Kostylev, Appl. Phys. Lett. **90**, 092503 (2007).
[15] K. J. Kennewell, M. Kostylev, and R. L. Stamps, J. Appl. Phys. **101**, 09D107 (2007).
[16] Y. Nozaki, K. Tateishi, S. Taharazako, M. Ohta, S. Yoshimura, and K. Matsuyama, Appl. Phys. Lett. **91**, 122505 (2007).
[17] K. Y. Guslienko, S. O. Demokritov, B. Hillebrands, and A. N. Slavin, Phys. Rev. B **66**, 132402 (2002).
[18] The irradiation time of 1.3 s was chosen to accommodate for the analog electronics that controlled the rf switches. As demonstrated by other experiments such a long irradiation time does not increase the sample temperature significantly (see Ref. 3).
[19] This calculation is done in logarithmic scale. For such small values logarithmic and linear scale are almost identical.
[20] M. Donahue and D. G. Porter, National Institute of Standards and Technology Interagency Report NISTIR 6376, 1999, http://math.nist.gov/oommf/
[21] K. M. Lebecki, M. J. Donahue, and M. W. Gutowski, J. Phys. D **41**, 175005 (2008).
[22] The material parameters are $\mu_0 M_s = 1.08$ T (saturation magnetization), $A = 13 \times 10^{-12}$ J/m (exchange constant), and $\gamma = 176$ GHz/T (gyromagnetic ratio).
[23] M. P. Kostylev, A. A. Stashkevich, and N. A. Sergeeva, Phys. Rev. B **69**, 064408 (2004).
[24] G. Gubbiotti, S. Tacchi, G. Carlotti, P. Vavassori, N. Singh, S. Goolaup, A. O. Adeyeye, A. Stashkevich, and M. Kostylev, Phys. Rev. B **72**, 224413 (2005).
[25] L. D. Landau and E. Lifshitz, Phys. Z. Sowjetunion **8**, 153 (1935).
[26] C. Kittel, Phys. Rev. **73**, 155 (1948).
[27] K. Y. Guslienko and A. N. Slavin, Phys. Rev. B **72**, 014463 (2005).
[28] W. Scholz and S. Batra, J. Appl. Phys. **103**, 07F539 (2008).